Friction Modelling With Slip For Planetary Exploration Rovers

Stuart R.K. Shilliday
James Watt School of Engineering
University of Glasgow
Glasgow, UK
s.shilliday.1@research.gla.ac.uk

Sarah Swinton
James Watt School of Engineering
University of Glasgow
Glasgow, UK
s.swinton.1@research.gla.ac.uk

Salim Al Oufi
James Watt School of Engineering
University of Glasgow
Glasgow, UK
s.al-oufi.1@research.gla.ac.uk

Euan W. McGookin
James Watt School of Engineering
University of Glasgow
Glasgow, UK
euan.mcgookin@glasgow.ac.uk

Douglas G. Thomson
James Watt School of Engineering
University of Glasgow
Glasgow, UK
douglas.thomson@glasgow.ac.uk

Kevin J. Worrall
James Watt School of Engineering
University of Glasgow
Glasgow, UK
kevin.worrall@glasgow.ac.uk

***Abstract*—One of the more complex challenges to be overcome when modelling the dynamics of any mobile platform is the representation of the forces of friction. In this work, a verified friction model for a four-wheel planetary rover with skid steering is set out. The model is implemented in multiple simulation scenarios to cover the full scope of the rover's mobility (forward motion, turning, braking, and accelerating) in both 2D and 3D environments.**

***Index Terms*—mathematical modelling, friction, planetary exploration**

I. Introduction

Planetary exploration rovers (PERs) must operate in remote and hazardous environments without access to a global positioning system. Such rovers are reliant on visual and wheel odometry to carry out accurate localisation [1]. Large localisation errors can be accumulated during motion due to the interaction of the rover's wheels and the terrain surface, which may result in performance degradation, or physical damage to the rover. For example, Ishigami et al. have shown the effect of slip on a rover's ability to follow a path along a slope [2]. Accurate modelling of the friction experienced by a PER is therefore beneficial when predicting the operational performance of the rover and ultimately the mission outcomes.

Friction modelling is often based on either wheel traction [3], [4], or vehicle dynamics [5]. When modelling wheel traction, the transfer of forces (both longitudinal and lateral) between the tyre and surface are considered. The wheel traction method requires calculation of the rotational and translational velocities of the wheel to be able to approximate the friction coefficient, which is based on the slip between the wheel and the contact surface. The vehicle dynamics method investigates the rigid body dynamics of the vehicle. However, when modelling the friction through vehicle dynamics, the wheel slippage is not considered. Previous work at the University of Glasgow set out a validated model for a four-wheel rover [5], using an actuator model to generate torques which acted directly on the dynamic model, without considering the intermediate friction step. Recent work by Isermann sets out a comprehensive description of the physical interaction of the wheel with the ground [3]. However, this model is primarily implemented for traditional automotive designs, not fixed, skid steering rovers. By modelling the wheel/surface interaction in more detail, the initial stages of terramechanics [6], that is the dynamic interaction between the ground and the wheel, can be included in the model.

While other work on slip-based friction modelling for PERs focuses on either kinematic models [7] or passive suspension rover platforms [8], the contribution of this work is to implement friction in a light-grey-box, non-linear, dynamic model of a rigid-chassis PER. Presented herein is a verified friction model for a four-wheel planetary rover, on a rigid surface, with skid steering which generates turning motion by applying differential voltages to each side of the rover. The development of this friction model and verification by comparison with a previously validated model is outlined in this paper as follows. Section II describes the mathematical model of the rover's dynamics and control system. Section III sets out the developed friction model. Verification results are presented in Section IV and the conclusions drawn from this work are discussed in Section V.

II. Four-Wheel Rover Model

The mathematical model of a four-wheel rover that used in this work contains the kinematics and the rigid-body dynamics of a Lynxmotion 4WD rover [5]. Firstly, two frames of reference define the kinematics in this model (Fig. 1): the Earth-fixed frame, and the rover body frame.

The rover's equations of motion, with reference to the rover body-fixed frame and Earth-fixed frame, are described by the matrix relationships shown in Equation (1) [9].

This document is the result of the research project funded by the Engineering and Physical Sciences Research Council and the Saudi Government.

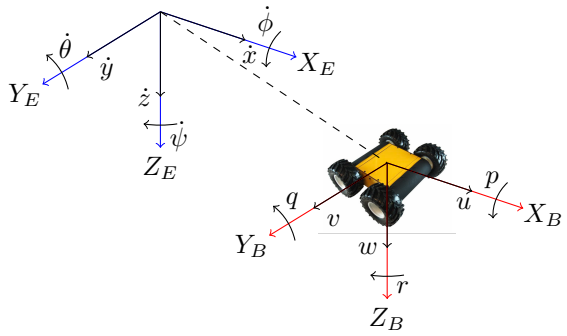

Fig. 1. Earth-fixed (X_E, Y_E, Z_E (blue)) and rover body-fixed axes (X_B, Y_B, Z_B (red))for the modelled four wheel Lynxmotion rover

$$\begin{aligned} \boldsymbol{M}\dot{\boldsymbol{\nu}} + \boldsymbol{C}(\boldsymbol{\nu})\boldsymbol{\nu} &= \boldsymbol{\tau} - \boldsymbol{D}(\boldsymbol{\nu}) - \boldsymbol{g}(\boldsymbol{\eta}) \\ \dot{\boldsymbol{\eta}} &= \boldsymbol{J}(\eta)\boldsymbol{\nu} \end{aligned} \tag{1}$$

In the above equation, $\boldsymbol{\nu}$ is the body-fixed velocity vector, $\boldsymbol{\eta}$ is the inertially fixed position/orientation vector, $\boldsymbol{M}$ is the mass and inertia matrix, $\boldsymbol{C}(\boldsymbol{\nu})$ is the Coriolis matrix, $\boldsymbol{D}(\boldsymbol{\nu})$ is the damping matrix, $\boldsymbol{g}(\boldsymbol{\eta})$ represents the gravitational forces and moments, $\boldsymbol{J}(\boldsymbol{\eta})$ is an Euler matrix representing the trigonometric transformation from the body fixed reference frame to the earth fixed reference frame, and the $\boldsymbol{\tau}$ vector represents the reactive frictional forces and moments that arise from the action of the actuators. Throughout this work, the front left, back left, front right, and back right rover wheels are indexed as n = 1, 2, 3, and 4, respectively.

A. Unbalanced Forces

The right hand side of Equation (1) comprises the unbalanced force and moment terms for each of the 6 degrees of freedom of the rover. There are three primary sources for each of these terms; air resistance, gravity, and friction. The first two of these are formulated as shown by Worrall [5].

The air resistance is only considered in the surge direction as, under nominal operating conditions, the velocity of the rover in the other directions is negligible. This force component acts as a damping term, resisting the motion of the rover and is proportional to the square of the rover's surge velocity.

The centre of gravity and the origin of the body-fixed reference frame are coincidental, and consequently, there is no moment generated by the action of gravity on the rover. The magnitude of the gravitational force in each of the three translational axes is dependent on the rover roll, pitch, and yaw angles (ϕ, θ, and ψ) as seen in Equation (2), where g is the acceleration due to gravity.

$$\boldsymbol{g}(\boldsymbol{\eta}) = \begin{bmatrix} -m.g.\sin(\theta) \\ -m.g.\sin(\phi).\cos(\theta) \\ m.g.\cos(\phi).\cos(\theta) \\ 0 \\ 0 \\ 0 \end{bmatrix} \tag{2}$$

It is worth noting that the gravitational force in the Z axis is completely counteracted by the reaction force provided by the surface that the rover is driving on. This reaction force is also significant in the calculation of friction forces. Friction is the third and final source for the external forces and moments acting on the rover. A detailed explanation of how these forces are generated is given in Section III.

B. Model Structure

The rover model operates with two primary subsystems: the actuators and the general rigid body equations of motion. The equations of motion have been set out in Section II, and the actuators are modelled as electromechanical DC motors, as are used in the Lynxmotion rover [10].

The motors are provided with voltage inputs by the control system, and produce corresponding rotational velocities for the wheels, ω. These rotational velocities allow the friction model to generate forces that drive the rover rigid body model.

C. Control and Guidance System

The rover's guidance system is modelled using a Line-of-Sight (LOS) algorithm. A PID controller is implemented for surge velocity and a PD controller is implemented for heading. The navigation, guidance and control systems are implemented as represented by Ireland et al [10]. Fig. 2 shows the guidance, navigation and control system for the rover, where ψ and ψ_d are the measured and desired heading, respectively. The rover's measured position is denoted by x and y, and its measured and desired velocities are $\vec{v}$ and $\vec{v}_d$, respectively.

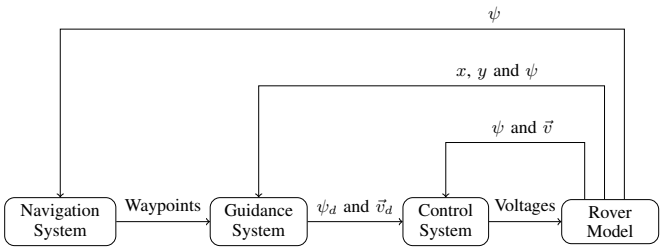

Fig. 2. PER guidance, navigation and control system

III. Friction Model

Any force generated by the wheels of the rover occurs due to the interaction of the tyre and the driving surface, when there exists a relative velocity between the tyre contact point and the driving surface [3]. Therefore, friction is the source of both propulsive and resistive forces. The motor model provides a rotational velocity, ω, of the wheel, which is used as an input to the friction model.

Fig. 3 shows the velocity components generated within the model, where u_{wc} and v_{wc} are the surge and sway velocities of the wheel centre point, respectively. Therefore, $\vec{v}_{wc}$ is the resultant velocity of the wheel centre, which is rotated from the surge axis by the sideslip angle of the wheel, α. The friction model requires an accurate calculation of the tangential velocity of the tyre at the contact point between the wheel and the ground, u_{tan}. In Fig. 3, u_{wc} is greater than u_{tan}, therefore the wheel is rotating slower than its translational motion, and the rover is braking.

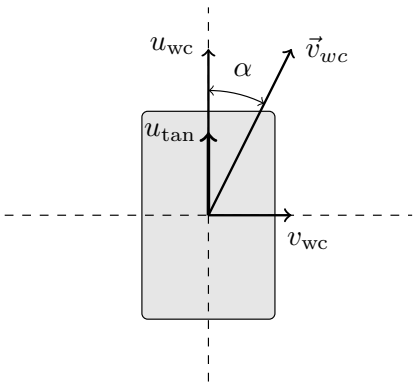

Fig. 3. Components of velocity due to interaction between the rover wheel and the driving surface

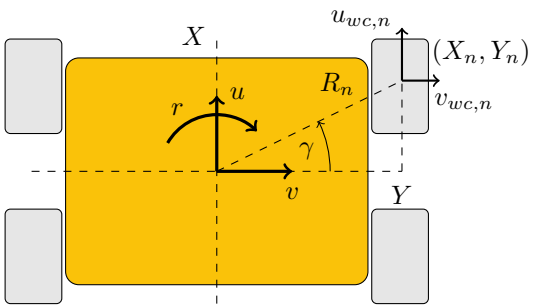

Fig. 4. Velocity components of the rover

A. Vertical Wheel Forces (Weight Distribution)

As the rover experiences longitudinal and lateral accelerations, the vertical forces applied to each of the rover wheels vary. Vertical wheel forces F_{ZT} for each one of the four wheels are distributed as in Equation (3).

$$F_{\mathrm{ZT}} = m.g.\cos(\theta).\cos(\phi)[K_1 \quad K_2 \quad K_3 \quad K_4]^T \tag{3}$$

where m is the mass of the rover, g is the gravitational acceleration, θ and ϕ are pitch and roll angles, and K_{n} is the weight distribution ratio for each wheel and is calculated using Equations (4) and (5).

$$\begin{aligned} K_1 &= K_{front}K_{left} \\ K_2 &= K_{rear}K_{left} \\ K_3 &= K_{front}K_{right} \\ K_4 &= K_{rear}K_{right} \end{aligned} \tag{4}$$

$$\begin{aligned} K_{front} &= \frac{l_r}{L} - \frac{h}{L}\left(\tan(\theta) + \frac{a_X}{g.\cos(\theta)}\right) \\ K_{rear} &= \frac{l_f}{L} + \frac{h}{L}\left(\tan(\theta) + \frac{a_X}{g.\cos(\theta)}\right) \\ K_{left} &= \frac{1}{2} - \frac{h}{w}\left(\tan(\phi) + \frac{a_Y}{g.cos(\phi)}\right) \\ K_{right} &= \frac{1}{2} + \frac{h}{w}\left(\tan(\phi) + \frac{a_Y}{g.\cos(\phi)}\right) \end{aligned} \tag{5}$$

where h is the height of centre of gravity of the rover, w is the width of the rover, a_x the longitudinal acceleration, a_y the lateral acceleration, and l_r and l_f are the rear and front moment arm, $L = l_r + l_f$.

B. Wheel Centre Velocity

The rover's surge, sway, and yaw velocities must be taken into account to calculate the wheel centre velocities. Fig. 4 shows the coordinate reference frame of the rover and the wheel, and the wheel centre velocities generated by the combination of the rover surge u, sway v, and yaw r. Equation (6) calculates the longitudinal wheel centre velocity, $u_{\mathrm{wc,n}}$, and the lateral wheel centre velocity, $v_{\mathrm{wc,n}}$, respectively.

$$\begin{aligned} u_{\mathrm{wc,n}} &= u - R_n.r.\cos(\gamma) \\ v_{\mathrm{wc,n}} &= v + R_n.r.\sin(\gamma) \end{aligned} \tag{6}$$

From the rover geometry, this equation can be simplified using the relationships $X_n = R_n.\sin(\gamma)$ and $Y_n = R_n.\cos(\gamma)$, giving the equations shown in Equation (7).

$$\begin{aligned} u_{\mathrm{wc,n}} &= u - r.Y_{\mathrm{n}} \\ v_{\mathrm{wc,n}} &= v + r.X_{\mathrm{n}} \end{aligned} \tag{7}$$

C. Slip

The longitudinal slip of the rover wheel is defined as the absolute difference between the longitudinal wheel centre velocity and the tangential velocity resulting from the wheel's rotation, i.e. $u_{tan} = r_W.\omega$. This slip is then normalised to give the longitudinal slip coefficient, S_x, as shown in Equation (8). This equation holds for driving and braking states and nominally the value for S_X will be between 0 and 1, however it exceeds 1 if the wheel is counter rotating with respect to the direction of travel of the rover.

$$S_X = \frac{|u_{wc} - r_W\omega|}{max(|u_{wc}|, |r_W\omega|)} \tag{8}$$

Similarly, lateral slip is defined as the relative velocity of the ground with respect to the tyre surface, and since there is no tangential component from the rotation of the wheel, this is simply the wheel centre lateral velocity. Once again, this is normalised to give Equation (9).

$$S_Y = \frac{|v_{wc}|}{max(|u_{wc}|, |r_W\omega|)} \tag{9}$$

The slip components S_X and S_Y are then combined to give a resultant slip as in Equation (10), from which the friction coefficient can be evaluated.

$$S_{res} = \sqrt{S_X^2 + S_Y^2} \tag{10}$$

D. Friction Coefficient

The friction coefficients are defined as the ratio of the lateral or longitudinal forces to the vertical load through the wheel, as shown in Equation (11) [3]. This relationship allows the lateral and longitudinal forces to be calculated from the vertical forces. These vertical forces are calculated using the weight distribution set out in section III-A.

$$\mu_{XT} = \frac{F_{XT}}{F_{ZT}}$$
$$\mu_{YT} = \frac{F_{YT}}{F_{ZT}} \tag{11}$$

The friction coefficients are functions of several variables, including slip, surface conditions, and sideslip angle. Several methods of modelling this behaviour are discussed by Isermann [3]. Fig. 5 shows a comparison of five friction coefficient modelling methods [11].

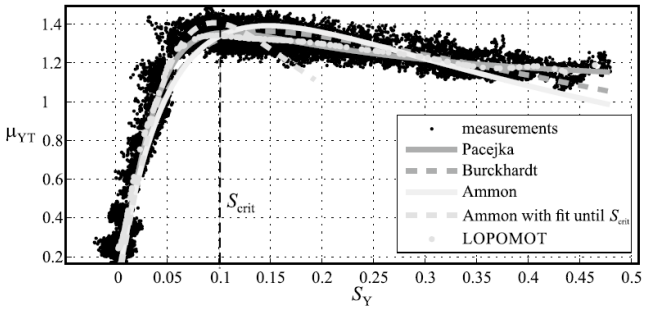

Fig. 5. Lateral friction coefficient values with respect to lateral slip [11]

The model that has been deemed, for this work, to most accurately track the behaviour of the μ is Pacejka's 'Magic Formula' [12], shown in Equation (12). This is because it is the model that best tracks the friction coefficient at large values of slip.

$$\mu = \mu_{max}.\sin(C.\tan^{-1}(B.S - E(B.S - \tan^{-1}(B.S)))) \tag{12}$$

$$E = \frac{B.S_{crit} - \tan(\frac{\pi}{2.C})}{B.S_{crit} - \tan^{-1}(B.S_{crit})} \tag{13}$$

In the above equation, μ_{max} is the maximum value reached by the friction coefficient, S is the slip ratio, B is a constant that determines the gradient of the slope at $S = 0$, C is a constant that defines the behaviour of the friction coefficient after the maximum, and E is a form coefficient that ensures that μ_{max} occurs at S_{crit}, as shown in Equation (13).

Similarly to the slip ratio, a resultant coefficient can be used to combine both μ_{XT} and μ_{YT}. In this case the equations for the longitudinal and lateral frictional forces are as shown in Equation (14). In these equations, k_y is an attenuation factor which, according to Kiencke and Nielsen [13], normally falls within the range of 0.8-0.95.

$$F_{XT} = \mu_{res}.F_{ZT}.\frac{S_X}{S_{res}}$$
$$F_{YT} = k_y.\mu_{res}.F_{ZT}.\frac{S_X}{S_{res}} \tag{14}$$

These forces, once calculated, can be included in the dynamics of the rover model with their relative directions assigned. The longitudinal force changes direction depending on whether the tangential tyre velocity is greater than the wheel centre velocity or not. The lateral force always acts in opposition to the direction of the lateral wheel centre velocity.

E. Aligning Torque

The lateral tyre force does not necessarily act through the centre of the tyre contact patch, and in fact acts slightly behind it by a distance known as the caster offset [3]. This causes a restorative aligning torque, M_{ZT} as shown in Fig. 6.

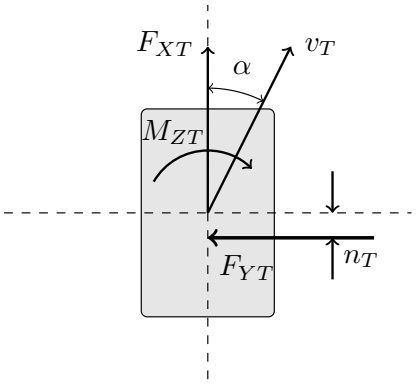

Fig. 6. Aligning torque caused by caster offset

The caster offset, n_T, is typically a function of both the vertical load through the wheel, and the sideslip angle [3].

F. Dynamics

The longitudinal and lateral forces and the aligning torque all combine to operate on the rigid rover body and generate accelerations in the respective surge, sway, and yaw directions. The surge and sway components sum to give the total frictional force in each direction, as shown in Equation (15).

$$F_{xf} = \sum_{i=1}^{4} F_{XT,i}$$
$$F_{yf} = \sum_{i=1}^{4} F_{YT,i} \tag{15}$$

The moment caused by friction about the yaw axis is less trivial to calculate. Since the lateral and longitudinal forces can be asymmetric through each of the wheels, they do not necessarily cancel and both components must be taken into consideration. The moment calculation is as shown in Equation (16), where Equations (17), (18), and (19) are the moments generated by the surge force, sway force, and aligning torque respectively. The X_i and Y_i terms are the longitudinal and lateral distances of the wheel centre from the centre of gravity respectively.

$$M_{zf} = M_{surge} + M_{sway} + M_{yaw} \tag{16}$$

$$M_{surge} = -\sum_{i=1}^{4} F_{XT,i}.Y_i \tag{17}$$

$$M_{sway} = \sum_{i=1}^{4} F_{YT,i}.X_i \tag{18}$$

$$M_{yaw} = \sum_{i=1}^{4} M_{ZT,i} \tag{19}$$

The environments considered in this work all assume a perfectly planar surface, so it can be assumed that, although the rover chassis is rigid, there are no instances where any of the wheels might leave the surface and cease to contribute to the forces and moments in the dynamic model.

IV. Results

Three test cases have been considered: 2D straight line following, 2D closed loop waypoint following, and 3D closed loop waypoint following. This test set encompasses the full scope of the rover's mobility (forward motion, turning, braking, and accelerating) in both 2D and 3D environments.

A. 2D Straight Line

For the initial straight line simulation scenario, the rover's motors are supplied with a series of voltages, which are changed once every five seconds. All four motors receive the same voltage at each step. Fig. 7 shows the rover tyre velocities and tangential wheel velocities of each wheel for straight-line motion with varying input voltages as per Table I.

TABLE I
INDEX OF EACH ROVER WHEEL

Time Segment (s)	Voltage Applied (V)
[0,5]	10
[5,10]	6
[10,15]	2
[15,20]	0
[20,25]	-2
[25,30]	-6
[30,35]	-10
[35,40]	0

It can be seen from Fig. 7 that the wheel centre velocities follow the same stepwise behaviour as the voltages, which is to be expected. Notably there is an overshoot at each of the steps, caused by the implementation of the wheel as a load on the motors. More important, however, is the fact that the wheel centre and tangential tyre velocities are almost identical, meaning that the slip, while necessary for any longitudinal forces to be generated, is minimised in the steady state.

The validated Lynxmotion model created by Worrall [5], referred to here as the torque model, has been used as a comparison metric. For this model, although the motor models are identical, the armature current in the motor is directly transformed into torques that are applied to the rigid-body model. This effectively bypasses the wheel, the slip, and the consequent friction considerations. Viscous friction is then added at a later point. The resultant rover velocity of both models are shown in Fig. 8.

Two features immediately apparent in the performance of the torque model are the higher velocities attained by the rover, and the lack of overshoot. The missing overshoot can be explained simply by the fact that, as mentioned previously, the current-to-torque transformation bypasses the wheel-motor interaction, and hence removes the torsional stiffness of the motor shaft as a consideration in the model behaviour. The difference in velocities suggests that further validation of the friction slip model is required, but the similarity in general behaviour verifies that the model is performing as expected.

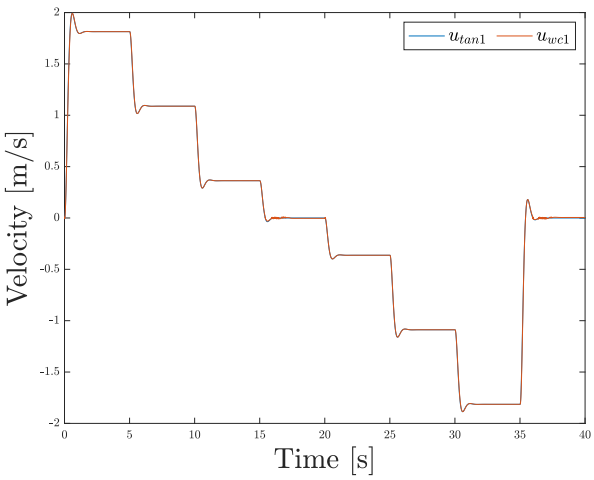

Fig. 7. Rover tyre velocities and tangential wheel velocities of each wheel for straight line motion with varying input voltages

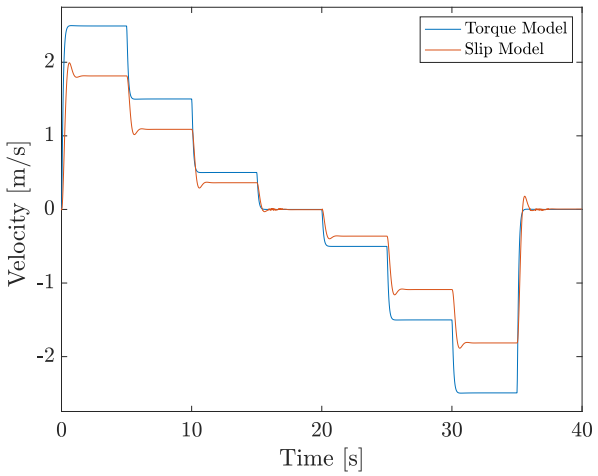

Fig. 8. Comparison of velocity response of torque and slip models to voltage inputs

B. 2D Closed Loop Waypoint Following

In order to test the turning motion of the rover, a closed loop control system was implemented, and a series of waypoints were supplied, such that the rover follows a serpentine path. Fig. 9 shows the rover tyre velocities and tangential wheel velocities of each wheel for this manoeuvre.

These plots show that the closed loop control successfully generates differential drive voltages to cause the rover to turn

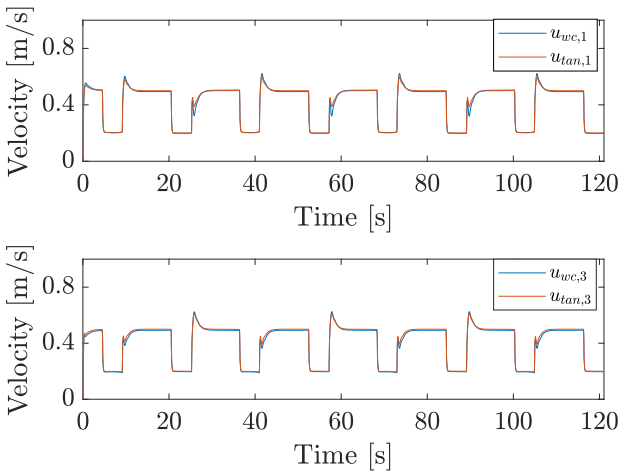

Fig. 9. Rover tyre velocities and tangential wheel velocities of each wheel for 2D closed loop waypoint following

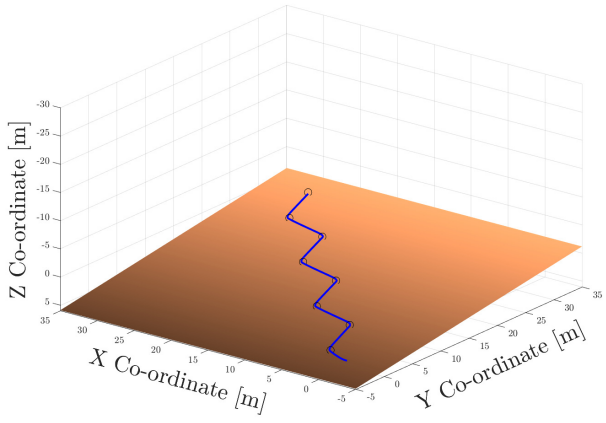

Fig. 10. Serpentine path of the rover. Each waypoint is shown by a black circle, and the rover path is shown in blue

before returning to steady-state constant values. There is also evidence of instances where the tangential tyre velocities differ from those of the wheel centres, indicating that there is an increased slip when the rover is attempting to turn. This follows logically, as the opposing forces of the wheels on either side of the rover increases the tendency of each side to slip slightly as the turn manoeuvre is being performed.

C. 3D Closed Loop Waypoint Following

Fig. 10 shows the path of the rover as it successfully follows its waypoints within a 3D environment with a slope angle of 10°. The differences between the 2D and 3D cases of the tyre and tangential wheel velocities are negligible, showing a robustness of the friction model and rover control system for the slope angle considered.

Further investigation showed that the friction model successfully allows the rover to follow these waypoints up to an angle of 30°, which is greater than Curiosity's absolute operational limit [14]. This limit is therefore deemed to be acceptable, and the model satisfactory.

The previously developed torque model was validated for multiple 2D cases, but when implemented in a 3D simulation, the sideslip angle increases exponentially, and the model breaks down. The response shown in Fig. 10 shows that the increased fidelity of the slip model developed in this work allows it to perform closer to expected behaviour than the torque model.

V. Conclusions

Accurate modelling of the friction experienced by a PER is important for creation of an accurate high fidelity model. This work investigates a verified friction model for a four-wheel planetary rover with skid steering. This model has been implemented within various simulation scenarios to cover the full scope of the rover's mobility (forward motion, turning, braking, and accelerating) in both 2D and 3D environments, successfully verifying the behaviour of the friction and slip model by comparison with a previously validated model. It has been shown that including the wheel traction mechanism within the rover model allows for similar performance for 2D simulations, and increases the operational envelope to include 3D environments when compared to the torque model.

References

[1] Sasaki T, Otsu K, Thakker R, Haesaert S, Agha-mohammadi Aa. Where to map? Iterative rover-copter path planning for mars exploration. IEEE Robotics and Automation Letters. 2020;5(2):2123-30.

[2] Ishigami G, Nagatani K, Yoshida K. Path following control with slip compensation on loose soil for exploration rover. In: 2006 IEEE/RSJ International Conference on Intelligent Robots and Systems. IEEE; 2006. p. 5552-7.

[3] Isermann R. Automotive control: modeling and control of vehicles. Springer; 2022.

[4] Ahn CS. Robust Estimation of Road Friction Coefficient for Vehicle Active Safety Systems.; 2011.

[5] Worrall KJ. Guidance and search algorithms for mobile robots: application and analysis within the context of urban search and rescue. University of Glasgow; 2008.

[6] Muro T, O'Brien J. Terramechanics. CRC Press; 2004.

[7] Rabiee S, Biswas J. A friction-based kinematic model for skid-steer wheeled mobile robots. In: 2019 International Conference on Robotics and Automation (ICRA). IEEE; 2019. p. 8563-9.

[8] Yoshida K, Hamano H. Motion dynamics and control of a planetary rover with slip-based traction model. In: Unmanned Ground Vehicle Technology IV. vol. 4715. SPIE; 2002. p. 275-86.

[9] Fossen TI. Guidance and control of ocean vehicles; 1994.

[10] Ireland ML, Worrall KJ, Mackenzie R, Flessa T, McGookin E, Thomson D. A Comparison of Inverse Simulation-Based Fault Detection in a Simple Robotic Rover with a Traditional Model-Based Method; 2017. p. 607-15.

[11] Bauer M. Methoden zur modellbasierten Fahrdynamikanalyse und Bewertung von Fahrdynamikregelsystemen. VDI Verlag GmbH; 2015.

[12] Pacejka H. Tire and vehicle dynamics. Elsevier; 2005.

[13] Kiencke U, Nielsen L. Automotive control systems: for engine, driveline, and vehicle. IOP Publishing; 2000.

[14] Rankin A, Maimone M, Biesiadecki J, Patel N, Levine D, Toupet O. Driving curiosity: Mars rover mobility trends during the first seven years. In: 2020 IEEE Aerospace Conference. IEEE; 2020. p. 1-19.